Smart Structures and Systems, *Vol. 28, No. 3 (2021) 355-362*
https://doi.org/10.12989/sss.2021.28.3.355

A multi-physics informed antenna sensor model through the deep neural network regression

Chunhee Cho [1a], LeThanh Long [2b], JeeWoong Park [3c] and Sung-Hwan Jang*[4d]

[1] *Department of Civil and Environmental Engineering, University of Hawaii at Manoa, Honolulu Hawaii, USA*
[2] *Information Technology Department, Duy Tan University, Da Nang, Vietnam*
[3] *Department of Civil and Environmental Engineering and Construction, University of Nevada at Las Vegas, Las Vegas, Nevada, USA*
[4] *Department of Civil and Environmental Engineering, Hanyang University (ERICA Campus), Ansan-si, Kyngkido, Korea*

(*Received September 14, 2020, Revised March 18, 2021, Accepted May 15, 2021*)

Abstract. A passive wireless strain sensing method using antenna sensors has significantly advanced structural health monitoring systems. Since the dimensions of antenna sensors are sensitive to their strain sensing performance and operating frequency, an iterative tuning process is required to achieve a final optimized design. Although multi-physics finite element simulation enables accurate estimation of antenna performance for each turning iteration, the simulation process requires high computational resources. Therefore, antenna tuning processes are recognized as obstacles to delay the final design process. In this study, we explore the potential of multi-physics informed models as an alternative approach for analyzing antenna sensors. Through deep neural networks, as a branch of the machine-learning algorithms, we formulate multi-physics informed models with six input parameters (antenna dimensions) and two outputs (resonance frequency and strain sensitivity). Twenty-two hundred high fidelity data sets are prepared by simulating multi-physics models: 1,600, 400, and 200 data sets are applied to deep neural network regression (DNNR) training, validating, and testing, respectively. From extensive data investigation, an optimized DNNR architecture is obtained to be two layers, with 16 neurons in each layer. Its training, validating, and testing values of mean square errors are 13.01, 44.22, 37.27, respectively. Finally, the proposed multi-physics informed model predicts the resonance frequency and strain sensitivity with errors of 0.1% and 0.07%, respectively. In addition, since the average computation speed for each tuning process is 0.007 seconds, the practical usefulness of the proposed method is also proven.

Keywords: antenna strain sensor; deep neural network; machine learning; multi-physics simulation; patch antenna; wireless strain measurement

1. Introduction

The main concept of structural health monitoring (SHM) research is based on the idea that structural conditions, including safety, are directly or indirectly presented by analyzing operating conditions and structural responses, such as strain, displacement, acceleration, humidity, and temperature (Sohn *et al*. 2003). Among the various measurands needed for SHM, strain is one of the most important indicators, representing stress concentration and damage development. Therefore, strain sensing technologies have received attention, and researchers have developed many types of strain sensors, such as metal foil strain gages, vibrating wire sensors, and fiber optic sensors (Chang and Güemes 2013, Derkevorkia *et al*. 2017). Although the performance of these sensors is adequate in many applications, most of the sensors require a cabled system for data acquisition and power supply. However, cabled systems can be costly, not only in system installation, but also in long-term system maintenance (Çelebi 2002, Huo *et al*. 2017). To overcome expensive cabled monitoring systems, wireless sensor nodes have been developed for several decades (Sohn *et al*. 2003). Wireless sensing devices generally consist of three functional modules: sensing interface, computing core, and wireless communication. However, most wireless sensing devices usually operate on an external power source, such as batteries.

As an alternative approach to achieve wireless strain measurement, antenna strain sensors have been developed to monitor strain concentration in structures (Yi *et al*. 2011, 2013, and 2014, Li and Wang 2020, Zhang *et al*. 2018, Tchafa and Huang 2019). Antenna strain sensors adopt passive wireless communication, which does not require any power source on the sensor side. The strain sensing mechanism of the antenna sensor is considered with two physical domains between electromagnetics and mechanics. Because an antenna strain sensor is bonded on a structural surface, the antenna strain sensor deforms together with the structure when uncertain loading is applied. Such structural deformation affects the change of electromagnetic properties, which shifts the resonance frequency of the antenna sensor. By measuring resonance frequency change

*Corresponding author, Assistant Professor,
E-mail: sj2527@hanyang.ac.kr
[a] Assistant Professor, Ph.D., E-mail: chunhee@hawaii.edu
[b] Associate Professor, P.D.,
E-mail: lethanhlong@dtu.edu.vn
[c] Assistant Professor, Ph.D., E-mail: jee.park@unlv.edu

ISSN: 1738-1584 (Print), 1738-1991 (Online)

using a reader antenna, the wireless strain measures can be estimated. To properly design an antenna stain sensor, numerical simulation techniques for electromagnetics have been developed for several decades. Antenna simulation methods mainly include the finite difference time domain (FDTD) method (Yee 1966, Taflove 1988), multiresolution time-domain method (MRTD) (Yee 1966), finite element method (FEM) (Taflove 1988, Bushyager and Tentzeris 2005) finite integration technique (FIT) (Volakis *et al*. 1998), and method of moment (MOM) (Ney 1985, Adam 1974). Antenna sensor design, and its performance prediction are usually achieved using commercial software packages specialized in electromagnetics, such as HFSS (High Frequency Structural Simulator), CST (Computer Simulation technology), and ADS (Advanced Design System). However, these software packages are specialized in solving only electromagnetic problems and cannot add other simulations of physical domains (e.g., mechanics) required for antenna sensor simulation under strain effects.

In order to accurately describe antenna sensor behavior involving mechanics and electromagnetics, multi-physics coupled simulation is inevitable (Cho et al. 2016, Lopato and Herbko 2018, Balanis 1989). In the multi-physics domain, mechanical simulation analyzes the deformed shapes of an antenna sensor and moving meshes provide a link that transfers the mechanical simulation results (strain and displacement) to an electromagnetic simulation. Then, a frequency domain solver runs the electromagnetic simulations and identifies the resonance frequency under different strain levels. Because the strain sensitivity and resonance frequency of an antenna sensor are sensitive to the sensor dimensions, an iterative tuning process is usually required to optimize the strain sensing performance of the antenna sensor. Thus, iterative multi-physics simulations require changing sensor dimensions. However, although the simulation results are accurate, by involving two physical domains (mechanics and electromagnetics), the computation process is more complicated. As a result, the entire design process requires high computational costs and efforts, which are major obstacles to improving the design of antenna strain sensors.

To address this issue, a multi-physics informed model, with the aid of deep neural network regression (DNNR), as a branch of deep learning methods (DL), is developed to effectively calculate the strain sensitivity and resonance frequency of an antenna sensor. As input of the ML training, the antenna dimensions are formulated with a vectorized format. According to each input, multi-physics simulations are conducted to generate high fidelity data. Although the nature of multi-physics simulation generates a lot of physical parameters, due to connecting multiple physical domains, most of the parameters are unnecessary for estimating the strain sensing performance of an antenna sensor. Therefore, only two factors, strain sensitivity and resonance frequency, are extracted as output for the DNNR training, validating, and testing data.

The rest of this paper is organized as follows. Section 2 presents the strain sensing mechanism of the antenna sensors. Section 3 explains the antenna sensor design and its numerical analysis method, which is a multi-physics finite element method (FEM), by integrating two physical domains between mechanics and electromagnetics. Section 4 formulates the multi-physics informed model realized by the DNNR. The formulated multi-physics models are trained, validated, and tested in Section 5. Finally, the paper is summarized with a conclusion and future work.

2. Strain sensing mechanism of an antenna sensor

An antenna sensor enables researchers to perform wireless strain sensing by recognizing resonance frequency change. Once an antenna sensor is bonded on a structural surface for strain measurement, the sensor deforms together with the structure, as shown in Fig. 1(a). The resonance frequency, $f_{\mathrm{R0}}^{\mathrm{Patch}}$, of a patch antenna is formulated as the following Eq. (1) (Balanis 1989).

$$f_{\mathrm{R0}}^{\mathrm{Patch}} = \frac{c}{2(L+L')\sqrt{\beta_{\mathrm{reff}}}} \tag{1}$$

where c is the speed of the light, L is the physical length of the copper cladding on the antenna, β_{reff} is the effective dielectric constant of the antenna substrate, and L' is the additional electrical length due to the fringing effect. Because the thickness-to-width ratio of a patch antenna is much smaller than one, the effective dielectric constant β_{reff} has approximately the same value as the dielectric constant β_{r0} (Balanis 1989)

$$\beta_{\mathrm{reff}} = \frac{\beta_{\mathrm{r0}}+1}{2} + \frac{\beta_{\mathrm{r0}}-1}{2}\left[1+12\frac{h}{W}\right]^{-1/2} \cong \beta_{\mathrm{r0}} \tag{2}$$

where h and W are the thickness and width of the substrate, respectively; and β_{r0} is the relative dielectric constant of the substrate, which is the intrinsic value dielectric material.

As shown in Fig. 1(a), when a structural surface is deformed by a certain loading condition, the patch antenna deforms together. As a result, the length of the electrical path for the surface current is also changed. If strain ε occurs in the longitudinal direction, the resonance frequency is shifted, as Eq. (3)

$$f_{\mathrm{R}}^{\mathrm{Patch}} = \frac{c}{2(1+\varepsilon)(L+L')\sqrt{\beta_{r0}}} = \frac{f_{\mathrm{R0}}^{\mathrm{Patch}}}{1+\varepsilon} \tag{3}$$

By Taylor expansion, Eq. (3) is represented as Eq. (4).

$$f_R^{Patch} = f_{\mathrm{R0}}^{\mathrm{Patch}}(1-\varepsilon+\varepsilon^2-\varepsilon^3+\varepsilon^4-\varepsilon^5+\cdots) \tag{4}$$

Generally, SHM focuses on measuring small strain levels that are usually less than a few thousand micro-strain levels. Therefore, the resonance frequency of the sensor changes approximately linearly with respect to strain, as Eq. (5)

$$\begin{aligned} & f_{\mathrm{R0}}^{\mathrm{Patch}}(1-\varepsilon+\varepsilon^2-\varepsilon^3+\varepsilon^4-\varepsilon^5+\cdots) \\ \cong\ & f_{\mathrm{R0}}^{\mathrm{Patch}}(1-\varepsilon) \end{aligned} \tag{5}$$

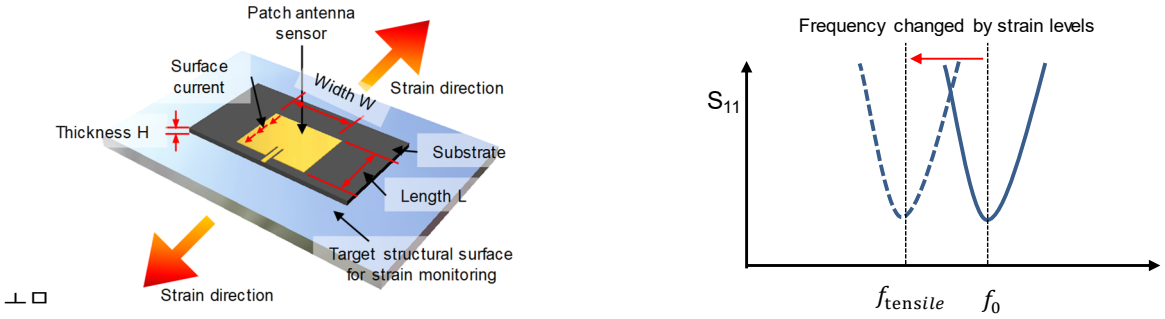

(a) Illustration of a patch antenna sensor (b) Frequency change by strain

Fig. 1 Strain sensing mechanism of antenna sensor

Based on this linear relationship, a strain level can be estimated by measuring the shift in the antenna resonance frequency. This serves as the fundamental strain sensing mechanism of the wireless antenna sensor. Fig. 1(b) illustrates the relationship between sensor deformation and antenna resonance frequency. When strain ε is positive, the current path is elongated. Therefore, the resonance frequency f decreases according to Eq. (5). On the other hand, if strain ε is negative, the resonance frequency f increases.

3. Multi-physics simulation for analyzing antenna sensors

In order to clearly understand the strain sensing performance of an antenna sensor, a 2.9 GHz patch antenna is modeled as an example, using the commercial multi-physics software package COMSOL (COMSOL 2020) (Fig. 2). At the center of the air sphere, the patch antenna is on an aluminum plate. The material of the microstrip patch is copper and its planar dimension is 44.5 mm × 33.3 mm, with a thickness of 0.7874 mm. The substrate material is Rogers RT/duriod®5880, with dielectric constant (ε_r = 2.2) and low loss tangent of 0.0009. For the mechanical simulation setup, strain is applied to the two ends of the aluminum specimen from zero to 2,000 με, with 500 με per step. As the 3D full-wave electromagnetic simulation is setup, perfect electrical conductor (PEC) boundaries are assigned to the outside of the air sphere and the ground plane. The 50 Ohm port is installed at the end of the micro-strip to feed electromagnetic waves. Since the designed resonance frequency is 2.9 GHz, the frequency sweeping range is set from 2,880 MHz to 2,920 MHz. The perfect matched layer (PML), which is assigned to the outside of the air sphere, mimics free space by absorbing the

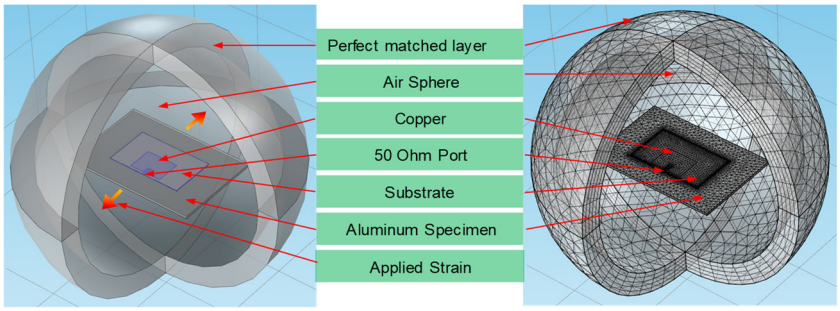

Fig. 2 Multi-physics simulation model (coupling mechanics and electromagnetics simulation)

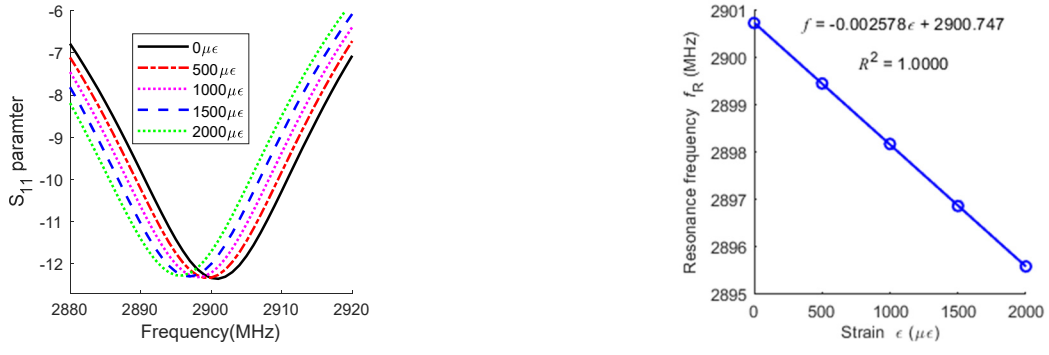

(a) S_{11} parameter (b) Resonance frequency versus strain

Fig. 3 Simulation results

electromagnetic wave. Namely, the PML boundary truncates the electromagnetic simulation domain. The total number of degrees of freedom (DOFs) is 259,975. Simulations are conducted on a desktop with an Intel® Core ™ processor i7-8700 (3.2 GHz 6-core) and 16 GB RAM memory.

For mechanical simulation, different assigned strain levels are applied for each step. Moving meshes transfer deformed shapes to the electromagnetic simulation. A frequency domain solver simulates a scattering parameter S_{11}, which is defined by the voltage ratio between the input and output. When the value of S_{11} closes to the minimum, the antenna has the highest radiation performance. At that time, the corresponding frequency is called the resonance frequency. As shown in Fig. 3(a), the computation of an S_{11} curve at each strain level is performed for 51 frequency points, consuming 17,892 seconds (4 hours, 58 minutes, 12 seconds) in total. While the strain level increases, the S_{11} curves move from right to left, including resonance frequencies.

As a post processing procedure, linear regression is performed with those minimum data points (resonance frequencies) to construct a strain sensitivity plot that presents multi-physical domains, as shown in Fig. 3(b). While the X-axis indicates strain levels in the mechanical domain, the Y-axis presents corresponding resonance frequencies in the electromagnetic domain. Finally, the resonance frequency is 2,900.75MHz at zero strain, and the strain sensitivity is –2,578 Hz/με, which means a 1 με strain experienced by the patch antenna introduces a frequency change of –2,578 Hz. The coefficient of determination is close to 1.0, which shows a highly linear relationship.

4. Formulation of multi-physics informed model by integrating deep neural network regression

4.1 Deep neural network regression

A neural network is named for biological neurons in humans, due to the similarity of their conceptual structures. To distinguish the neural network from real nerve cells, it is formally called, an artificial neural network (ANN) (Vapnik 1989 and Villarrubia *et al*. 2017). Due to the accuracy and the computational efficiency, various engineering areas adopts the ANN method to automate complicated process without extensive knowledge of statistics. By increasing the number of artificial neural units and layers, neurons are more complicated to each other, which is called a deep neural network (DNN), as shown in Fig. 4. Owing to the enhanced mathematical complexity, the architecture of a DNN enables researchers to improve the accuracy of prediction results. The DNN model consists of an input layer, an output layer, and multiple hidden layers. Each hidden layer contains artificial neuron units that have two functions: 1) the linear combination of input data with regulated weights; and 2) nonlinear complex functional mapping by activation functions, such as the sigmoid and the hyperbolic tangent functions. For forward propagation, the i^{th} hidden layer receives the input from the output of the $(i-1)^{th}$ hidden layer, and generates the output that is the input to the $(i+1)^{th}$ layer. On the contrary, backward propagation calculates the slopes of each layer through reverse order, and regulates their parameters.

A DNN model is categorized with two types: 1) classification and 2) regression. The main difference between the two depends on which activation functions of the last hidden layer and the output layer are applied. Classification problems utilize the nonlinear activation function at the last connection for binary classification (e.g., True: 1, False: 0), but a deep neural network regression (DNNR) replaces the activation function at the last hidden layer with a linear function to solve regression problems. Therefore, the DNNR model is a high-order regression function that enables researchers to predict continuous quantities of multi-physics behaviors through its mathematical complexities. After all, the DNNR model is suitable for developing a multi-physics informed model, and can be presented as in Eq. (6)

$$y_i = f_n\left(\cdots f_3\left(f_2\left(f_1(\boldsymbol{x}_i)\right)\right)\right) \tag{6}$$

where, x is the vectorized feature or data from the input layer (dimensions of an antenna sensor in this study); f_n is the neural network function of the n^{th} layer; y_i indicates the i^{th} prediction result in the output layer, which is strain

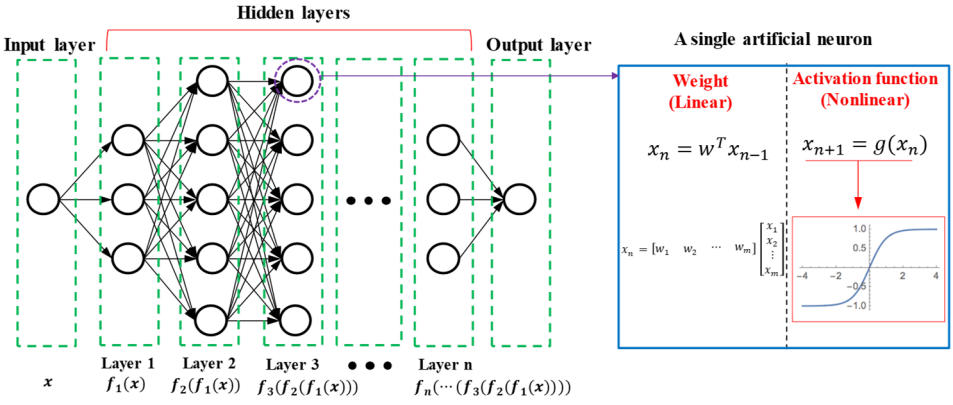

Fig. 4 Illustration of Deep Neural Network Regression (DNNR)

sensitivity and a resonance frequency. Finally, the training algorithm of the DNNR model is formulated as Eq. (7)

$$\underset{w}{\text{minimize}} \sum_{i=1}^{n} |y_i(\boldsymbol{w}, \boldsymbol{x_i}) - k_i| \tag{7}$$

where w is the weight matrix, n is the total number of training data sets, $\boldsymbol{x_i}$ is the i^{th} input data (dimensions of an antenna sensor), k_i is the corresponding output data (strain sensitivity and resonance frequency) to parameter x_i, and $\boldsymbol{w}$ represents the weight matrix in hidden layers.

4.2 Formulation of multi-physics informed model

The nature of DNNR is a black-box structure that is too complicated for humans to understand. However, the advantage of these mathematical complexities is enabling DNNR to formulate a multi-physics informed model that simulates the complicated behaviors of antenna sensors by considering two different physical domains between mechanics and electromagnetics. A key success factor for DNNR training (parameter regularization) is critically dependent on high fidelity datasets. Therefore, training, validating, and testing data sets are prepared with the aid of accurate multi-physics simulation, as shown in Fig. 5.

Once the substrate material and its patch antenna sensor thickness are confirmed, the dimensions of the patch antenna have an important role to determine the strain sensing performance (strain sensitivity) and resonance frequency. Since the antenna sensor is supposed to operate within ultra-high frequency (UHF) bands, the aimed resonance frequency range is fixed from 2,700 MHz to 3,200 MHz. As shown in Fig. 5, the input vector is determined with six key tuning parameters based on the patch antenna design, and their initial values are set to

$$\boldsymbol{x}_0 = [2.40,\ 13.00,\ 1.30,\ 19.75,\ 9.50,\ 33.30]\text{mm} \tag{8}$$

With the initial parameters, the resonance frequency and strain sensitivity are 2,900.75 MHz and –2,578 Hz/με, respectively (reported in Figs. 2 and 3). Since a small input parameter change significantly affects strain sensitivity, as well as resonance frequency, the tuning range is set to ±15% from $\boldsymbol{x}_0$.

Fig. 5 summarizes the process of formulating a multi-physics informed model. First, 2,200 input vectors are randomly generated within the defined range. Then the strain sensitivity and resonance frequency for each input are accurately analyzed through a multi-physics simulation tool in order to generate outputs (resonance frequency and strain sensitivity). Finally, the DNNR is trained with prepared input and output data sets. Iterative improvements are made to the physics-informed model by comparing the results of the multi-physics simulation.

5. Results

To formulate the physics-informed model through DNNR training, 2,200 data sets are prepared; 1,600, 400, and 200 data sets are applied to the DNNR training, validating, and testing, respectively. For processing multi-physics informed models, a commercial software package, MATLAB (developed by MathWorks) is adopted (MATLAB 2019). Multi-physics informed models with different DNNR configurations are formulated to search for the optimal architecture of layers and neurons. The first configuration starts with one hidden layer consisting of eight neurons. The number of neuron units and hidden layers are gradually increased until optimal results are obtained. For the optimal search, ten DNNR configurations of the multi-physics informed model are investigated, as summarized in Table 1.

In order to find the best performance, each configuration is executed for DNNR training and validating 100 times (multi-start approach), and 1,000 epochs are set as the maximum number of iterations. Learning performances are evaluated by comparing training, validating, and testing mean square errors (MSEs), which are calculated as the following Eq. (9)

$$\text{MSE} = \frac{1}{n}\sum_{i=1}^{n}(Y_i^{\text{Simulation}} - Y_i^{\text{DNNR}})^2 \tag{9}$$

where n is the total number of data; $Y_i^{\text{Simulation}}$ is the vectorized output at the i^{th} data set that contains resonance

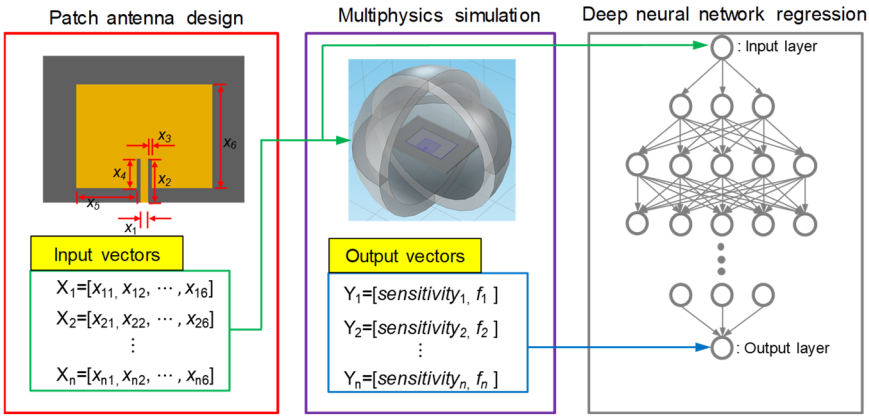

Fig. 5 Schematic of physics-informed model for antenna sensor design

Table 1 Neural network architecture configurations to search the optimal solution

Layer configuration		1st	2nd	3rd	4th	5th	6th	7th	8th	9th	10th
Number of layers		1	1	1	2	2	2	2	2	2	3
Number of neurons	1st layer	8	16	32	8	8	16	16	16	32	8
	2nd layer				4	8	4	8	16	32	8
	3rd layer										8
Training MSE		81.03	59.00	33.78	57.30	46.17	32.85	21.67	13.01	2.14	27.46
Validating MSE		99.10	66.35	45.11	58.39	51.28	54.14	55.84	44.22	131.64	54.29
Testing MSE		92.94	67.44	42.09	61.11	57.93	51.28	50.59	37.24	111.69	54.77

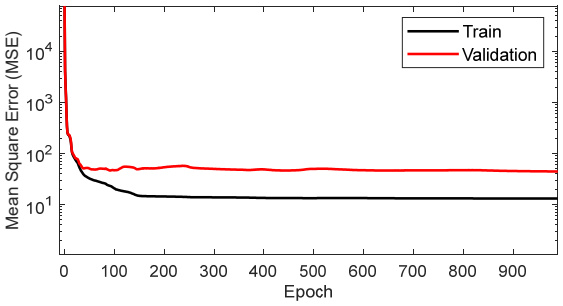

Fig. 6 DNNR performance comparisons for each epoch

frequency and strain sensitivity simulated from multi-physics coupled solutions; and Y_i^{DNNR} is the corresponding prediction result from the multi-physics informed model formulated by the DNNR.

As shown in Table 1, while gradually increasing layers and neurons (increasing the number of configurations), the values of the MSEs decreased. The smaller MSE estimated, the higher predicting performance is expected. After all, the eighth configuration (2 layers with 16 + 16 neurons) is selected as the optimized architecture because its MES values are relatively smaller than the other configurations. Although the ninth configuration (2 layers with 32 + 32 neurons) has the smallest value of training MSE, its validating and testing MSEs are higher than 100. In other words, the DNNR training of the ninth configuration is overfitted. In addition, more neurons are added in the ninth configuration, which causes it to be computationally inefficient and redundant.

To visually present the updated DNNR performance of the eight configuration, Fig. 6 plots training and validating MSE values as a result of the iterative process. After the DNNR performances are effectively updated from zero to 50 epochs, training and validating MSEs are converged to 13.01 and 44.22, respectively. After optimizing the multi-physics informed model through DNNR training, the prediction performances regarding resonance frequency and strain sensitivity are tested with 200 data sets. The value of testing MSE is 37.24 and the prediction details are shown in Figs. 7(a) and (b). Each prediction takes 0.007 seconds, and the average prediction errors for resonance frequency and strain sensitivity are 0.1% and 0.07%, which indicate high

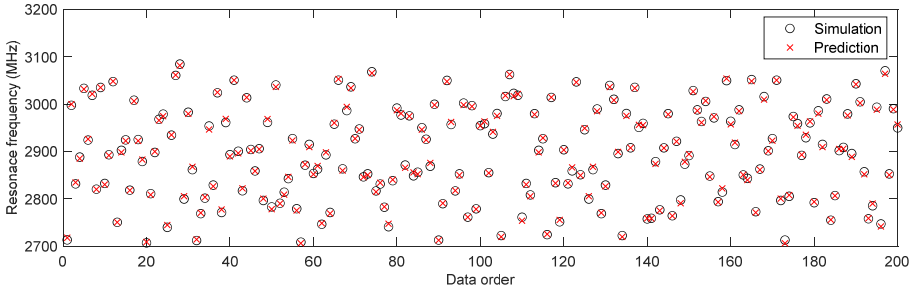

(a) Prediction of resonance frequency

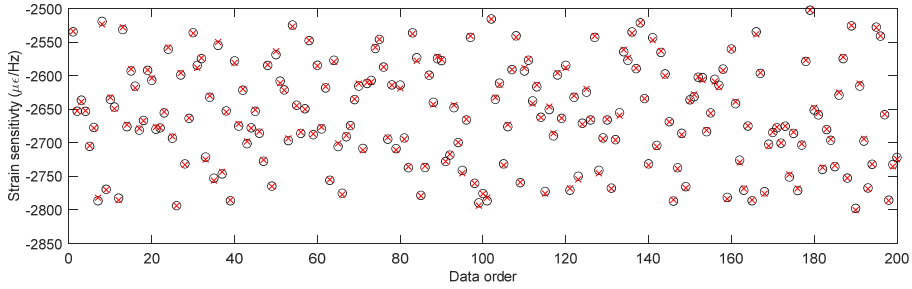

(b) Prediction of strain sensitivity

Fig. 7 Result comparison of the physics informed model and the multi-physics simulation model

accuracy. The average errors are calculated as the following Eq. (10)

$$\text{Error} = \frac{1}{n}\sum_{i=1}^{n}\left|\frac{Y_i^{\text{Simulation}} - Y_i^{\text{DNNR}}}{Y_i^{\text{Simulation}}}\right| \times 100 \qquad (10)$$

6. Conclusions

Among SHM technologies, an antenna strain sensor has the strong advantage of conveniently achieving wireless strain measurements for long term monitoring, in that the passive system does not require external batteries for sensing operations. The strain sensing mechanism of the antenna sensor is used to investigate electromagnetic property changes caused by mechanical deformation. Therefore, multi-physics simulation is inevitable to accurately predict strain sensing performance, by considering electromagnetics and mechanics. Especially, the tuning process requires iterative work to find an optimized antenna shape for strain sensing by changing sensor dimensions. However, although the accuracy of the multi-physics coupled simulation is high, slow computing speed is significant disadvantage to applying the multi-physics simulation to the tuning process.

To address this issue, a multi-physics informed model through DNNR was proposed in this study. To guarantee the prediction of strain sensing performance, high-fidelity data sets for DNNR processing were required. Therefore, 2,200 data sets were prepared through a multi-physics coupled FE simulation by changing six design tuning parameters; 1,600, 400, and 200 data sets were applied to DNNR training, validating, and testing, respectively. The nature of DNNR algorithms increases mathematical complexity by increasing the number of layers and artificial neurons. Such complex functional structures pursue a high accuracy of model prediction but require large computing resources. To avoid the computational redundancy of DNNR, ten configurations were formulated to search for the optimal architecture of layers and neurons by comparing MSE values. As a result, the eighth configuration (2 layers with 16 + 16 neurons) was selected as the most optimized architecture, and its training and validating MSE values were 13.02 and 44.22, respectively. As the final step to evaluate the formulated multi-physics model, the testing process was conducted and its average errors of predicting resonance frequency and strain sensitivities were 0.1% and 0.07%, respectively. Finally, the authors proved the proposed method: that multi-physics informed models were able to predict the resonance frequency and strain sensitivity of antenna strain sensors, including practical usefulness.

In spite of the achievements of this work, there are still limitations to be addressed in future research. To prove the proposed idea in advance, the authors tried to minimize the number of tuning parameters, and did not consider other parameters, such as substrate thickness or dielectric constants, which may affect final strain sensing performances. In addition, although the formulated DNNR model immediately predicted resonance frequency, and with high accuracy, the model was too mathematically complicated for engineers (users) to understand and did not provide any physical information about how to estimate specific parameters. This black-box nature of a complex DNNR algorithm is a concern for further practical applications in SHM. Therefore, a future study will involve a deeper level of investigation on these subjects, which will cover more general cases of antenna sensor design through ML study with big data, as well as develop DNNR interpreters to uncover the internal mechanism of the trained neural networks to determine how they arrive at a particular prediction.

Acknowledgments

This work was supported by the research fund of Hanyang University (HY-2020-N).

References

Adams, A.T. (1974), “An introduction to the method of moments”, *Comput. Phys. Commun.*, **68**(1), 1-18. https://doi.org/10.1016/0010-4655(91)90191-M

Balanis, C.A. (1989), *Advanced Engineering Electromagnetics*, New York: Wiley & Sons, Inc.

Bushyager, N.A. and Tentzeris, M.M. (2005), *Multi resolution time domain method in electromagnetics*, Morgan & claypool, USA.

Çelebi, M. (2002), “Seismic instrumentation of buildings (with Emphasis on Federal Buildings)”, United States Geological Survey, Menlo Park, CA Report No. 0-7460-68170.

Chang, F.-K. and Güemes, A. (2013), “Structural heath monitoring 2013: a roadmap to intelligent structures”, Lancaster, PA, USA.

Cho, C., Yi, X., Li, D., Wang, Y. and Tentzeris, M.M. (2016), “Passive frequency doubling antenna sensor for strain and crack sensing”, *Sensors J., IEEE*, **16**(14), 5725-5733.

Cho, C., Yi, X., Li, D., Wang, Y. and Tentzeris, M.M. (2017), “An eigenvalue perturbation solution for the multi-physics simulation of antenna strain sensors”, *IEEE J. Multiscale Multiphys. Computat. Tech.*, **2**, 49-57. https://doi.org/10.1109/JMMCT.2017.2698338

Clemens, M. and Weiland, T. (2001), “Discrete electromagnetism with the finite integration technique”, *Progress in Electromagn. Res.*, **32**, 65-87. https://doi.org/10.2528/PIER00080103

COMSOL (2020), COMSOL multiphysics reference guide, COMSOL, Inc., Burlington, MA, USA.

Derkevorkian A., Pena, F., Masri, S. and Richards W. (2017), “Operation load estimation of chain-like structures using fiber optic strain sensors”, *Smart Struct. Syst., Int. J.*, **20**(3), 385-396. https://doi.org/10.12989/sss.2017.20.3.385

Huo, L., Li, X., Chen, D. and Li, H. (2017), “Structural health monitoring using piezoceramic transducers as strain gauges and acoustic emission sensors simultaneously”, *Comput. Concrete, Int. J.*, **20**(5), 595-603. https://doi.org/10.12989/cac.2017.20.5.595

Jin, J.M. (2002), The finite element method in electromagnetics, (2nd ed.), John Wiley & Sons, Inc., New York, USA.

Li, D. and Wang, Y. (2020), “Thermally-stable wireless patch antenna sensor for strain and crack sensing”, *Sensors*, **20**(14), 3835. https://doi.org/10.3390/s20143835

Lopato, P. and Herbko, M. (2018), “A circular microstrip antenna sensor for direction sensitive strain evaluation”, *Sensors*, **18**(1), 310. https://doi.org/10.3390/s18010310

MATLAB (2019), Natick, Massachusetts: The MathWorks Inc.

Ney, M.M. (1985), "Method of moments as applied to electromagnetics problems", *IEEE Transcations on Microwave Theory and techniques*, **33**(10), 972-980. https://doi.org/10.1109/TMTT.1985.1133158

Sohn, H., Farrar, C.R., Hemez, F.M., Shunk, D.D., Stinemates, D.W. and Nadler, B.R. (2003), "A Review of structural health monitoring literature: 1996-2001", Los Alamos National Laboratory, Los Alamos, NM Report No. LA-13976-MS.

Taflove, A. (1988), "Review of the formulation and applications of the finite-difference time-domain method for numerical modeling of electromagnetic wave interactions with arbitrary structures", *Wave Motion*, **10**(6), 547-582. https://doi.org/10.1016/0165-2125(88)90012-1

Tchafa, F. and Huang, H. (2019), "Microstrip patch antenna for simultaneous temperature sensing and superstrate characterization", *Smart Mater*. *Struct*., **28**, 105009. https://doi.org/10.1088/1361-665X/ab2213

Vapnik, V. (1995), *The nature of statistical learning theory*, Springer, New York, USA.

Villarrubia, G., Paz, J.F., Chamoso, P. and Prieta, F. (2017), "Artificial neural networks used in optimization problems", *Neurocomputing*, **272**(10), 10-16. https://doi.org/10.1016/j.neucom.2017.04.075

Volakis, J.L., Chatterjee A. and Kempel, L.C. (1998), "Finite element method for electromagnetics: with applications to antenna, microwave circuits, and scattering", The Institute of Electrical and Electronics Engineers, Inc., New York, USA.

Yee, K.S. (1966), "Numerical solution of initial boundary-value problems involving Maxwell's equations in isotropic media", *IEEE Transactions on Antennas and Propagation*, **14**, 302-307.

Yi, X., Wu, T., Wang, Y., Leon, R.T., Tentzeris, M.M. and Lantz, G. (2011), "Passive wireless smart-skin sensor using RFID-based folded patch antennas", *Int*. *J*. *Smart Nano Mater*., **2**(1), pp. 22-38. https://doi.org/10.1080/19475411.2010.545450

Yi, X., Cho, C., Cooper, J., Wang, Y., Tentzeris, M.M. and Leon, R.T. (2013), "Passive wireless antenna sensor for strain and crack sensing-electromagnetic modeling, simulation, and testing", *Smart Mater*. *Struct*., **22**(8), p. 085009. https://doi.org/10.1088/0964-1726/22/8/085009

Yi, X., Cho, C., Cook, B., Wang Y., Tentzeris, M.M. and Leon, R.T. (2014), "A slotted patch antenna for wireless strain sensing", *Proceedings of the ASCE 2014 Structures Congress*, Boston, MA, USA.

Zhang, J., Huang, B., Zhang, G. and Tian, G.Y. (2018), "Wireless passive ultra-high frequency RFID antenna sensor for surface crack monitoring and quantitative analysis", *Sensors*, **18**(7), 2130. https://doi.org/10.3390/s18072130

Zoeller, M. and Huber, M. (2019), "Survey on automated machine learning", arXiv preprint, arXiv: 1904.12054.